iScience

Article

Modeling hepatic steatosis with human adult stem cell-derived liver organoids

Graphical abstract

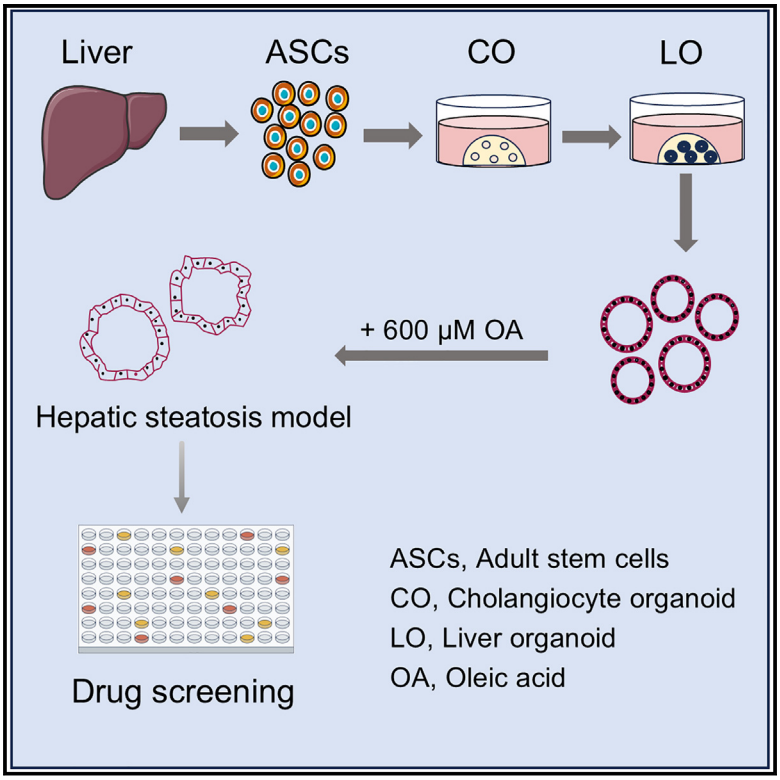

Highlights

- LOs displayed functional characteristics of mature hepatocytes
- LOs possessed potential for lipid metabolism
- Hepatic steatosis model of LOs could simulate steatosis and inflammation
- Hepatic steatosis model of LOs showed the potential of drug screening

Authors

Liuyang Zhu, Sen Liu, Ze Wang, ..., Tao Cui, Long Yang, Yamin Zhang

Correspondence

cuitao0909@126.com (T.C.), doctoryang321@163.com (L.Y.), 5020200824@nankai.edu.cn (Y.Z.)

In brief

Disease; Human metabolism; Cellular physiology; Stem cells research; Organizational aspects of cell biology; Specialized functions of cells

Zhu et al., 2025, iScience 28, 112344
May 16, 2025
https://doi.org/10.1016/j.isci.2025.112344

CellPress

iScience

CellPress
OPEN ACCESS

Article

Modeling hepatic steatosis with human adult stem cell-derived liver organoids

Liuyang Zhu,[1,8] Sen Liu,[2,8] Ze Wang,[3,8] Yueyue Yang,[4] Pinsheng Han,[5] Wen Tong,[1] Tianyu Zhao,[3] Libo Wang,[3] Tao Cui,[6,*] Long Yang,[7,*] and Yamin Zhang[7,9,*]

[1]First Central Clinical College of Tianjin Medical University, Tianjin 300070, China
[2]Department of Pharmacology, Shenyang Pharmaceutical University, Shenyang 110016, China
[3]State Key Laboratory of Druggability Evaluation and Systematic Translational Medicine, Tianjin Institute of Pharmaceutical Research, Tianjin 300000, China
[4]College of Life Sciences, Nankai University, Tianjin 300071, China
[5]Nankai University of Medicine College, Tianjin 300071, China
[6]Tianhui Biotechnology Co., Ltd., Hefei 230000, China
[7]Department of Hepatobiliary Surgery, Tianjin First Central Hospital, Tianjin 300192, China
[8]These authors contributed equally
[9]Lead contact
*Correspondence: cuitao0909@126.com (T.C.), doctoryang321@163.com (L.Y.), 5020200824@nankai.edu.cn (Y.Z.)
https://doi.org/10.1016/j.isci.2025.112344

SUMMARY

Metabolic dysfunction-associated steatotic liver disease (MASLD) remains the most common chronic liver disease worldwide, and appropriate *in vitro* models are of great significance for investigating pathogenesis and drug screening of MASLD. In this study, human expandable cholangiocyte organoids were derived from adult stem cells of normal liver tissue. After differentiation, liver organoids (LOs) exhibited the functional characteristics and genomic features of mature hepatocytes. To induce steatosis, LOs were incubated with a gradient concentration oleic acid, and it was found that the model could recapitulate the development of lipid accumulation and inflammation. In addition, the drug sensitivity of the hepatic steatosis model was further verified through anti-steatosis drug testing. In summary, LOs have great potential for disease modeling, and the results indicate that the hepatic steatosis model may serve as a useful tool for exploring the molecular mechanisms and drug screening of MASLD.

INTRODUCTION

Metabolic dysfunction-associated steatotic liver disease (MASLD) remains the predominant chronic liver condition globally, exhibiting a prevalence of around 25% that escalates in tandem with rising rates of obesity.[1,2] MASLD is characterized by metabolic stress-induced liver damage, intricately linked to insulin resistance and genetic predisposition.[3] The clinical spectrum of MASLD encompasses non-alcoholic hepatic steatosis, metabolic dysfunction associated steatohepatitis (MASH), cirrhosis, and hepatocellular carcinoma, emerging as a primary etiology of advanced liver disease and liver transplantation.[4,5] MASLD is associated with liver disease, disability, and mortality, as well as a heightened risk of metabolic syndrome, type 2 diabetes mellitus, atherosclerotic cardiovascular disease, and colorectal tumors.[6] The global prevalence of MASLD and MASH has resulted in significant health and economic challenges.

Lipid deposition-induced lipotoxicity is a major contributor to the development of metabolic disorders in MASLD.[7] Free fatty acids within the liver not only contribute to *de novo* lipid synthesis but also lead to lipotoxicity, metabolic disturbances, insulin resistance, and oxidative stress. These factors ultimately result in steatosis, hepatocyte injury, and apoptosis, thereby promoting the progression of MASLD.[8] The utilization of *in vivo* and *in vitro* models has progressively enhanced our comprehension of MASLD mechanisms. Large animal models, though more akin to human physiology, encounter constraints, such as ethical considerations and high processing expenses, curtailing their utility before clinical trials.[9] Therefore, rodent models of MASLD are mainly used to explore therapeutic targets, but species specificity and genetic constraints cannot be ignored to affect the potential response to drug therapy.[10] Moreover, although the 2D cell culture-based MASLD model remains prevalent, 3D cells culture technology, mimicking *in vivo* cellular interactions more closely, enhances model simulation.[11] Nevertheless, the models predominantly rely on immortalized cell lines or hepatocyte-like cells derived from pluripotent stem cells, lacking the precise genetic attributes and spatial organization of the human liver.[12,13] Hence, there is still an urgent demand for suitable and innovative models to facilitate mechanistic understanding of MASLD and developing therapeutics.

Recent years have witnessed significant advancements in liver organoids (LOs) research.[14] LOs derived from pluripotent stem cells exhibit the capability for prolonged *in vitro* expansion while maintaining genetic stability and are similar to the structural and functional attributes of liver *in vivo*.[15] Prior investigations have

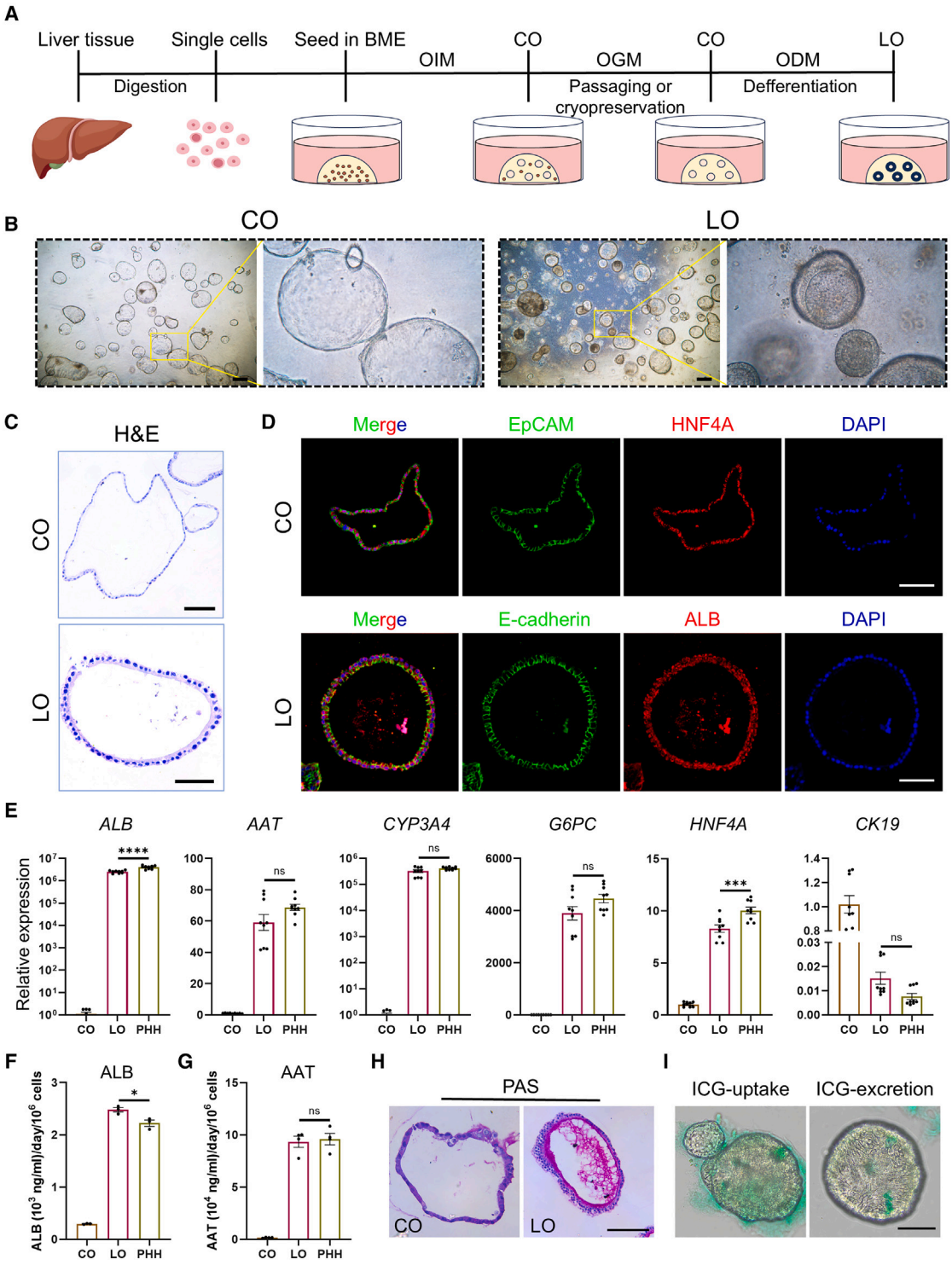

Figure 1. Generation and characterization of COs and LOs derived from ASCs of liver tissue

(A) Schematic diagram of the workflow of the COs derivation, COs expansion, and LOs differentiation. (BME, basement membrane extract; OIM, organoid initiating medium; OGM, organoid growth medium; ODM, organoid differentiation medium; CO, cholangiocyte organoid; LO, liver organoid).

(B) Representative images of generation of COs and LOs derived from ASCs. Scale bar, 200 μm.

(C) Morphological structure of the COs and LOs. Scale bar, 50 μm.

(D) Representative immunofluorescence images of EpCAM, HNF4A in COs and E-cadherin, ALB in LOs. Scale bar, 100 μm.

(E) mRNA expression levels of each specific markers in COs and LOs (3 cases of organoids derived from different patients, and n = 3/each case).

(legend continued on next page)

demonstrated that LOs derived from induced pluripotent stem cells (iPSCs), after incubation with free fatty acids, exhibit gene expression profiles akin to liver tissues from MASH patients, and recapitulate critical aspects of steatohepatitis, such as steatosis, inflammation, and fibrosis.[16–18] The Clever's team reported the successful expansion of bipotent cholangiocyte organoids (COs) from human adult stem cells (ASCs), which can differentiate into liver organoids *in vitro*.[19] Subsequent studies have utilized LOs derived from patients or mouse with MASH for personalized disease modeling and drug development, but the organoids exhibit slow growth and limited passages.[20,21]

Here, we developed a simple and efficient method to establish hepatic steatosis model. LOs differentiated from human expandable COs exhibited *in vivo* liver function and demonstrated lipid metabolism capabilities at the transcriptome level. After incubating with oleic acid (OA), the model recapitulated the development of hepatic steatosis characteristics and displayed sensitivity to anti-steatosis drugs. These promising results indicated that the hepatic steatosis model we constructed may be a useful tool for exploring the molecular mechanisms and drug screening of MASLD.

RESULTS

Expandable COs from liver tissue could differentiate into LOs

Firstly, we established the methodology for inducing LOs based on previous studies (Figure 1A). It was observed that the cells self-assembled to form COs after adding the organoid initiating medium (OIM) for 5–7 days, which exhibited a spherical and sac-shaped morphology (Figures 1B and 1C). The diameter of the organoids reaches about 1 mm on the 8-10th day and could be further purified after mechanical separation and passage with organoid growth medium (OGM). The COs exhibited rapid growth with a consistent passaging ratio of 1:4 to 1:6 every 3–5 days. Moreover, they demonstrated significant expansion potential following cryopreservation and recovery. Organoid differentiation medium (ODM) was added after 3 days of passage, and the lumen of spherical cystic organoids progressively darkened, accompanied by the emergence of polygonal cells resembling mature hepatocytes (Figures 1B and 1C).

LOs displayed histological and functional characteristics of mature hepatocytes

COs, commonly referred to as ductal organoids, possessed bidirectional differentiation capacity, able to differentiate into cholangiocytes and hepatocyte-like cells.[22] COs and LOs exhibited distinct tissue morphologies at the histological level. COs consisted of a single-layer epithelium, while LOs showed a thickened epithelium (Figure 1B). As markers of epithelial cells and stem cells, immunofluorescence results demonstrated that EpCAM, CK19, and SOX9 were expressed in COs, and the presence of HNF4A further suggested the potential for hepatocyte differentiation (Figures 1D and S1A). And mature hepatocyte markers such as albumin (ALB) and E-cadherin exhibited strong positivity in differentiated LOs (Figure 1D). And the LOs expressed high levels of liver-specific genes (such as *ALB*, *AAT*, *HNF4A*, *CYP3A4*, and *G6PC*), closed to those observed in primary hepatocytes (PHHs), whereas the expression of *CK19* was decreased in LOs compared to COs (Figure 1E). Furthermore, LOs displayed functional characteristics similar to mature hepatocytes. The differentiation process was accompanied by a gradual increase in the secretion of ALB and alpha-1-antitrypsin (AAT) (Figures S1B and S1C), and the levels of functional proteins secreted by differentiated LOs were comparable to those of PHHs (Figures 1F and 1G). Additionally, PAS staining revealed pronounced glycogen accumulation in LOs (Figure 1H), while the uptake and release of indocyanine green (ICG) was used to characterize the function of uptake, conjugation, and the subsequent release of the compounds like hepatocytes (Figure 1I).

Transcriptome analysis revealed the lipid metabolism capabilities of LOs

The expression levels of genes involved in lipid metabolism pathways were analyzed in LOs and COs, and the heatmap revealed that the key genes in these pathways were significantly up-regulated in the LOs compared to the COs. Furthermore, the elevated expression of these related genes was sustained even after multiple passages (Figure 2A). Accordingly, we conducted enrichment analysis on up-regulated differentially expressed genes (DEGs) in LOs. The Kyoto encyclopedia of genes and genomes (KEGG) pathway enrichment results showed that the up-regulated genes were mainly enriched in lipid metabolism-related pathways, including fatty acid degradation, fat digestion and absorption, and PPAR signaling pathway (Figure 2B). And gene ontology (GO) analysis results indicated that the up-regulated genes were mainly involved in lipid metabolic process, lipid transport, and fatty acid metabolic process (Figure 2C). Meanwhile, the gene set enrichment analysis (GSEA) analysis showed that the fatty acid metabolism and PPAR signaling pathway were identified in LOs (Figure 2D). In summary, the aforementioned results demonstrated that LOs possessed potential for lipid metabolism.

Hepatic steatosis model was induced from LOs with 600 μM OA

Preliminary results indicated that LOs have the liver functions and lipid metabolism capabilities of mature hepatocytes. To ascertain the optimal concentration of OA for the construction of hepatic steatosis model, LOs were subjected to incubation with gradient concentrations of OA ranging from 0 to 800 μM as previously reported. The results indicated that as the OA concentration increased, the lumen of the organoids darkened gradually in bright field, and Nile Red staining revealed a rise in lipid accumulation, as evidenced by an increase in Nile Red relative fluorescence intensity (Figure 3A; Figure S2A). ELISA analysis

(F and G) (F) ALB and (G) AAT production in the COs, LOs, and PHHs (n = 3).

(H) Representative images of PAS staining of COs and LOs. Scale bar, 100 μm.

(I) Representative images of LOs for the uptake and release of ICG. (ICG, indocyanine green) Scale bar, 100 μm. Results represent mean ± SD, ns, no significant difference, *p < 0.05, ***p < 0.001, and ****p < 0.0001. One-way ANOVA was used to compare between different groups.

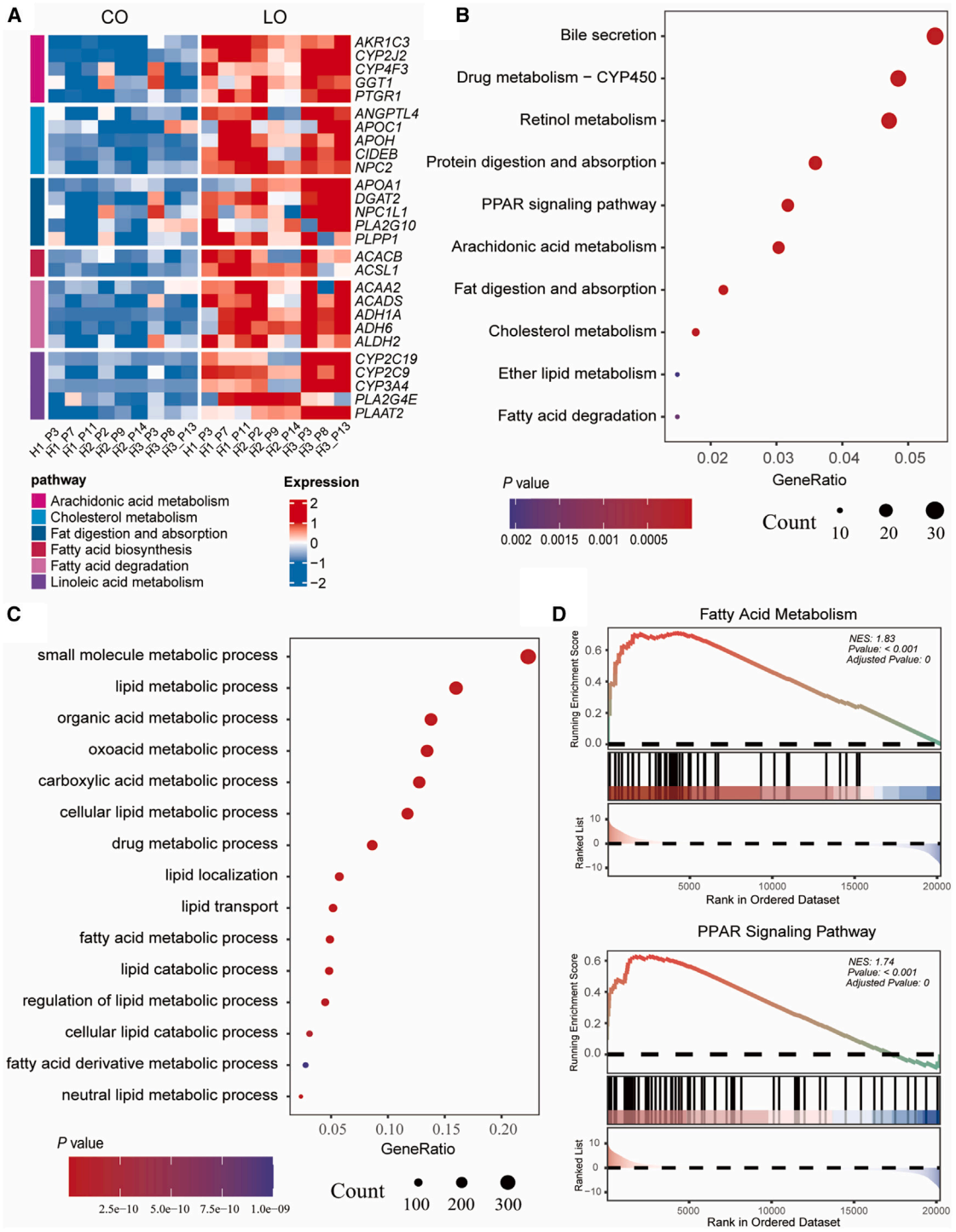

Figure 2. Transcriptome analysis of LOs revealed its capabilities of lipid metabolism

(A) Heatmap analysis of genes involved in pathways associated with lipid metabolism in COs and LOs. H1, H2, and H3 represented 3 cases of organoids derived from different patients. Px refered to the passage number of organoids.

(B) KEGG enrichment analysis for up-regulated genes in LOs.

(C) GO enrichment analysis for up-regulated genes in LOs.

(D) GSEA enrichment analysis showed the top-ranked subset signatures of hallmarks in LOs.

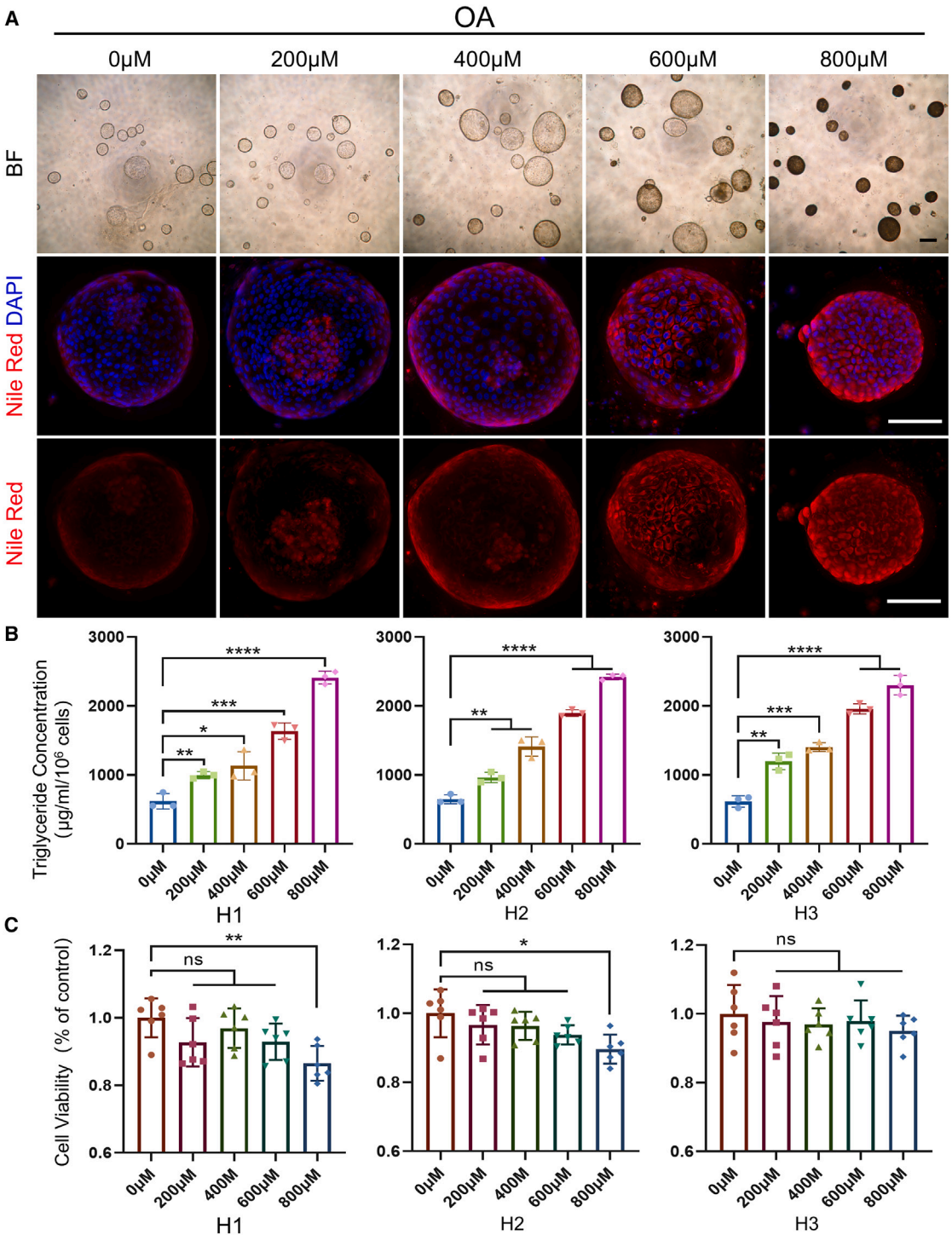

Figure 3. LOs were incubated with gradient OA to determine optimal concentration for hepatic steatosis model

(A) Representative images of LOs after incubating with gradient concentrations of OA for 3 days. Up: bright-field images of LOs, scale bar: 200 μm; middle and bottom: fluorescence images of LOs stained with Nile Red, scale bar, 50 μm.

(B) Quantitation of the triglyceride in LOs ($n = 3$) after incubating with gradient concentrations of OA for 3 days. H1, H2, and H3 represented 3 cases of organoids derived from different patients.

(C) Relative cell viability of LOs after incubating with gradient concentrations of OA for 3 days. H1, H2, and H3 represented 3 cases of organoids derived from different patients. Results represent mean ± SD, ns, no significant difference, $^{*}p < 0.05$, $^{**}p < 0.01$$^{***}p < 0.001$, and $^{****}p < 0.0001$. One-way ANOVA was used to compare between different groups.

confirmed that the gradient concentrations OA treatment resulted in a gradual elevation of triglycerides in the LOs derived from three patients, which constituted the primary components of lipid accumulation (Figure 3B). Moreover, cell viability measurement showed that gradually increasing concentrations of OA caused a slight decrease in cell viability in LOs. But at an OA concentration of 800 μM, 2 of 3 patient-derived LOs showed a significant decrease in cell viability (Figure 3C). Therefore, LOs were treated with 600 μM OA to establish the hepatic steatosis model.

Hepatic steatosis model replicated the steatosis and inflammation of MASLD

We had confirmed that significant lipid accumulation and elevated triglyceride content in LOs after incubating with 600 μM OA for 3 days. The expression levels of key genes involved in lipid metabolism, including the *de novo* lipogenesis related factors *SREBP*, the related enzyme *FASN*, and hepatic fatty acid translocase *CD36* were potently up-regulated in the hepatic steatosis model derived from three patients (Figure 4A). At the same time, the inflammatory factors *IL-6*, *IL-1β*, and *TNF-α* were also significantly up-regulated in the model, which was consistent with the result of ELISA of IL-6 (Figures 4A and 4B). H2DCFDA staining clearly demonstrated the positive of reactive oxygen species (ROS) in the model after treated with OA (Figure 4C). Furthermore, flow cytometry revealed a significantly higher proportion of ROS-positive cells in the steatosis model (65.03 ± 2.282% vs. 34.13 ± 3.346%, $p = 0.016$) (Figure 4D). These findings collectively suggested that LOs treated with OA successfully replicated the steatosis and inflammation characteristic of MASLD *in vitro*.

Drug testing revealed susceptibility of the model to anti-steatosis drugs

To assess the drug screening capabilities of the hepatic steatosis model, we evaluated the prophylactic or therapeutic effects of five anti-steatosis compounds. It could be observed that the color of organoids became lighter and Nile Red staining showed a significant reduction in lipid deposition after adding four drugs, including liraglutide, obeticholic acid, elafibranor, and saroglitazar (Figure 5A; Figure S2B). ELISA assays demonstrated a significant reduction in triglyceride content in LOs derived from three patients with anti-steatosis drugs tested, except for metformin. Among them, obeticholic acid and saroglitazar exhibited more substantial effects, reducing trilipid content in LOs by approximately 50% (Figure 5B). At the same time, treatment with four anti-steatosis drugs increased the cell viability of LOs (Figure 5C). However, metformin had no obvious effect on decreasing lipid accumulation and increasing cell viability. In addition, we noted that organoid steatosis models derived from different patients exhibited varied responses to drug therapy.

DISCUSSION

The lack of effective therapeutic agents for MASLD is partly due to the paucity of human-relevant models for target discovery and compound screening. And the rapid development of organoids has provided numerous innovative *in vitro* models for MASLD. A recent study utilized human fetal hepatocyte organoids to model the first stage of MASLD, specifically steatosis, through three different triggers: free fatty acid loading, interindividual genetic variability and monogenic lipid disorders.[23] Additionally, iPSCs-derived LOs have elucidated the known genotype-phenotype associations for MASLD, thereby facilitating the early identification and implementation of preventive and therapeutic strategies.[24] In this study, we established an *in vitro* model of hepatic steatosis by utilizing LOs differentiated from expandable COs. Human ASCs-derived LOs were used to recapitulate the pathophysiological changes of steatosis, including lipid accumulation and inflammatory response. Furthermore, the assessment of anti-steatosis drug responses using this steatosis model underscored its potential for drug screening applications.

MASLD is a chronic liver disease with a high clinical prevalence, closely associated with metabolic disorders, such as obesity, diabetes, and metabolic syndrome. It has emerged as a significant global health challenge, yet approved pharmacological treatments for MASLD and MASH remain elusive due to their complexity and phenotypic heterogeneity.[7] Recent advancements in *in vitro* and *in vivo* models have provided a variety of platforms for investigating MASLD pathogenesis and drug screening. Rat and mouse models have some advantages for studying MASLD, but experimental models of human origin are still essential given the obvious species barriers. In addition, *in vitro* models using HepG2, Huh7, and HepRG cell lines capture some features of MASLD in a 2D environment, but these immortalized malignant cells reduce the authenticity of the model, while the difficulty in maintaining and culturing primary hepatocytes limits their widespread application.[25]

The rapid progress in organoid technology has propelled research in various liver diseases, encompassing hereditary liver conditions, primary liver cancer, viral hepatitis, among others.[26] In this research, COs were induced from ASCs derived from normal liver tissues of three patients, following the method used by Clever's team.[19] It could be seen that ASCs exhibited self-assembly into COs about 3 days with OIM, and their stable passage and expansion capabilities conducive to generating substantial organoid quantities rapidly, which was also one of the crucial aspects for drug screening. These COs displayed characteristics of human bile duct epithelium, and have been used to construct drug-induced bile duct injury model and bile duct ischemia reperfusion injury model.[27,28] Moreover, bipotent COs exhibited the ability to differentiate into LOs *in vitro*, during which the ALB and AAT secretion were increased gradually. LOs expressed high levels of mature hepatocyte markers such as *ALB* and *CYP3A4*, and had glycogen accumulation and ICG uptake and release capabilities. And transcriptome analysis revealed the lipid metabolism capabilities of LOs. These aforementioned results indicated that the differentiated LOs had the genetic and functional characteristics of mature hepatocytes and could be used to construct MASLD models *in vitro*.

To induce steatosis, LOs were exposed to gradient concentrations of OA and, as we expected, the results increased lipid accumulation and triglyceride content as OA concentrations increased. Notably, 800 μM OA significantly compromised cell viability in the organoids, prompting the selection of 600 μM OA for inducing the steatosis model. In this model, lipid metabolism-related genes were increased, among which *SREBP*

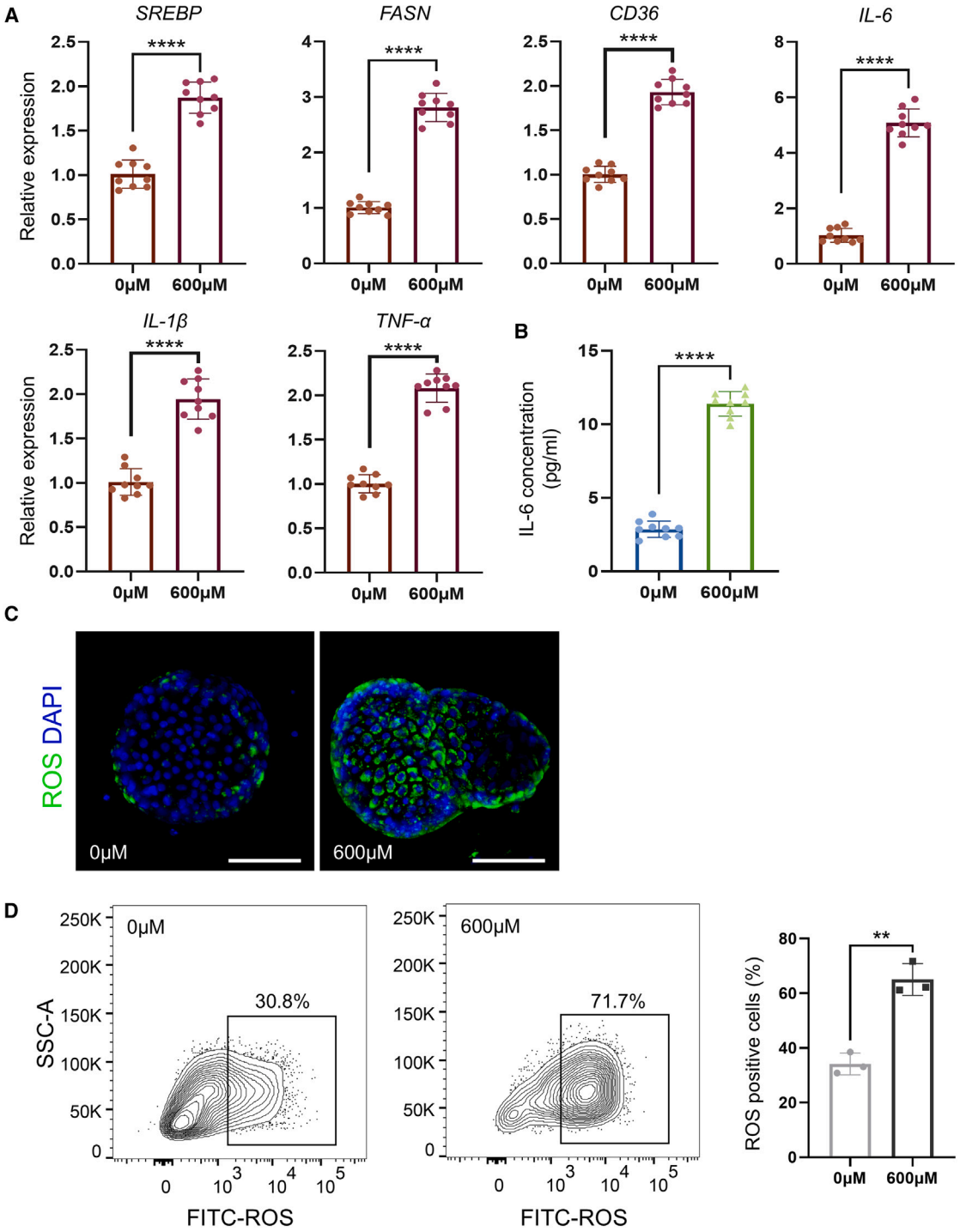

Figure 4. Modeling hepatic steatosis with LOs after incubating with 600 μM OA

(A) mRNA expression levels of specific genes associated with lipid metabolism and inflammation in the LOs with or without 600 μM OA (3 cases of LOs derived from different patients, and n = 3/each case).

(B) ELISA measurement of IL-6 in the LOs with or without 600 μM OA (3 cases of LOs derived from different patients, and n = 3/each case).

(C) Representative images of ROS staining in the LOs with or without 600 μM OA.

(D) Flow cytometry analysis to determine the proportion of ROS positive cells in LOs with or without 600 μM OA (n = 3).

Results represent mean ± SD, $^{**}p < 0.01$, $^{****}p < 0.0001$. t test was used to compare between two groups.

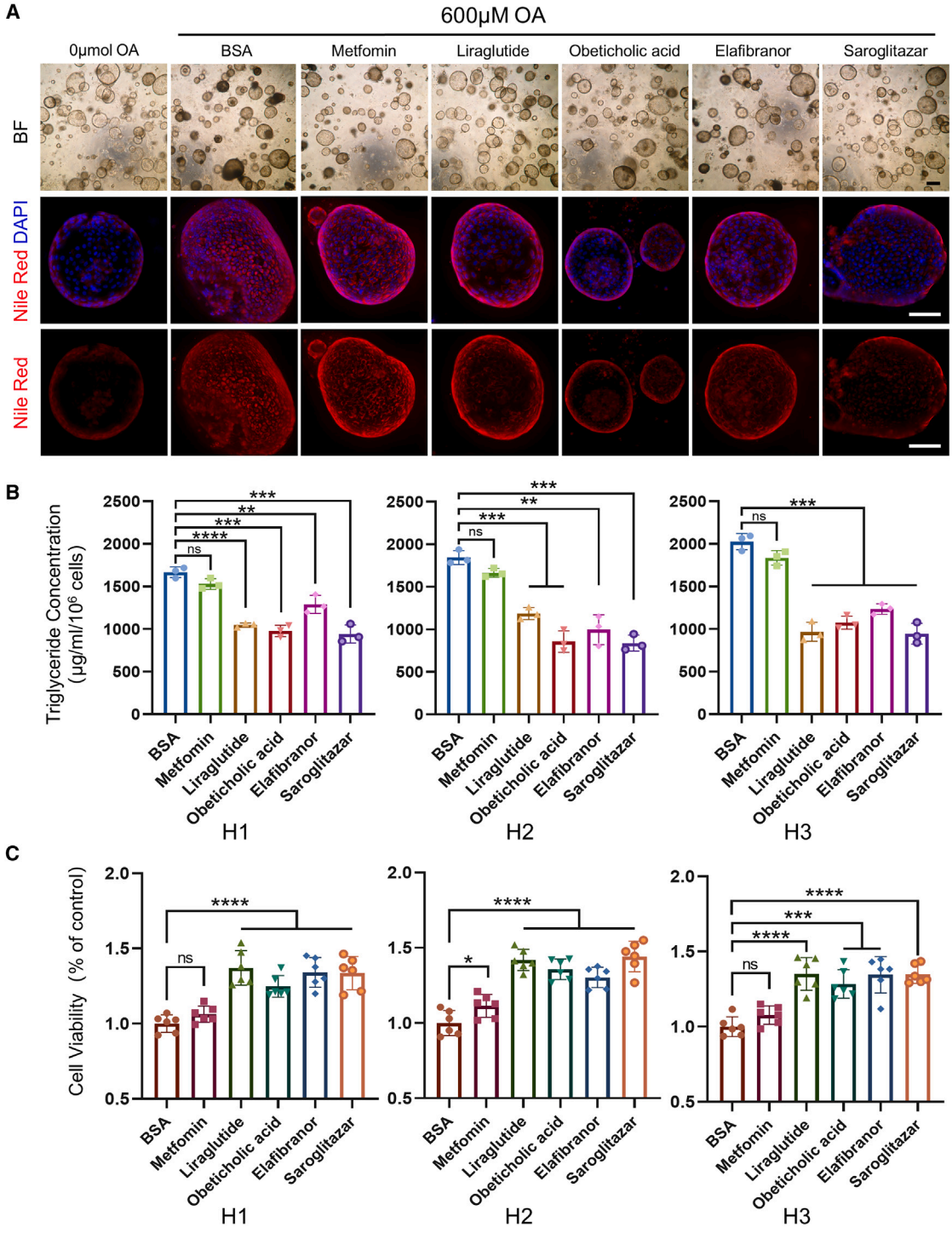

Figure 5. Hepatic steatosis model of LOs were used for drug screening

(A) Representative images of steatosis model of LOs after treatment with different drugs. Up: bright-field images, scale bar: 200 μm; middle and bottom: fluorescence images stained with Nile Red, scale bar, 50 μm.

(B) Quantitation of the triglyceride in steatosis model of LOs ($n = 3$) after treatment with different drugs. H1, H2, and H3 represented 3 cases of organoids derived from different patients.

(C) Relative cell viability of steatosis model of LOs ($n = 6$) after treatment with different drugs. H1, H2, and H3 represented 3 cases of organoids derived from different patients. Results represent mean ± SD, ns, no significant difference, $^{**}p < 0.01$, $^{***}p < 0.001$, and $^{****}p < 0.0001$. One-way ANOVA was used to compare between different groups.

was a major transcription factor in regulating genes involved in cholesterol, fatty acids, and triglyceride biosynthesis.[29] *FASN* was the key rate-limiting enzyme in fatty acid synthesis, while *CD36* dominated fatty acid transmembrane transport, and both genes played an important role in lipid metabolism.[30,31] Additionally, high expression of inflammatory factors and notably increased IL-6 secretion in the model mimicked the inflammatory response characteristic of MASH progression. Moreover, lipid metabolism disorders led to lipid accumulation, affecting different ROS generators, including mitochondria, endoplasmic reticulum, and NADPH oxidase, resulting in ROS overproduction.[32] Overall, these results suggested that our hepatic steatosis model reproduced the lipid accumulation and inflammatory response characteristics of MASLD *in vitro*.

To date, only resmetirom has been approved by the FDA for the treatment of MASH, but several drugs have been studied intensively or are entering clinical trials.[33,34] Appropriate *in vitro* models are of great significance for exploring drug mechanisms and drug screening. Therefore, we tested the therapeutic effect of several compounds to verify the drug screening capabilities of the hepatic steatosis model. Among them, metformin has been shown to have a role in preventing and alleviating liver steatosis, although its effectiveness remains a topic of controversy.[35] It could be seen that metformin didn't show anti-steatosis effect on the model in this study, which was consistent with previous report.[16] A recent study showed that metformin-induced TTP mediates communication between Kupffer cells and hepatocytes to alleviate hepatic steatosis by regulating lipophagy and necroptosis. The deficiency of macrophages and other stromal cells in LOs may be the reason for the weak anti-steatosis effect of metformin.[35] Four other drugs in clinical trials represent different drug classes and therapeutic targets and included agonists for the GLP-1 receptor (liraglutide), FXR (obeticholic acid), PPAR (elafibranor and saroglitazar).[36–38] The results showed that the model was sensitive to drugs, and the other four drugs showed significant anti-steatosis ability except metformin. Post-drug intervention, the model demonstrated reduced triglyceride content and enhanced cell viability, mirroring the drug screening potential observed in previous steatohepatitis models.[17,18] Interestingly, LOs models derived from distinct patients exhibited varied responses to drug therapy, underscoring individual differences in drug sensitivity, a critical consideration for drug evaluation and screening endeavors.

In conclusion, LOs have great potential for disease modeling with the functional characteristics and genomic features of mature hepatocytes. And the hepatic steatosis model in this study holds immense significance for deciphering the molecular mechanisms of MASLD, identifying therapeutic targets, and facilitating drug screening.

Limitations of the study

Establishing a hepatic steatosis model holds immense significance for deciphering the molecular mechanisms of fatty liver, identifying therapeutic targets, and facilitating drug screening.[39] However, there are still some limitations in this study. First, more ASCs-derived LOs are needed to construct hepatic steatosis models and to work with MASLD patient-derived LOs for the development of biomarkers or drug screening. Second, although LOs contain more physiological features of human organs than 2D hepatocytes, they lack vascular systems and other essential cell types, such as Kupffer cells and stellate cells, which are crucial for MASLD progression.[40,41] In addition, LOs has significant lipid metabolism-related genomic features compared with COs, however, its functional activity remained undetermined. Further biochemical and proteomic characterization will be critical to inform the significance of LOs related to the studies of hepatic lipid metabolism.[24] Moreover, hepatocyte-derived organoids exhibit functional and genomic characteristics that are more similar to mature hepatocytes, which may potentially serve as a valuable tool for constructing MASLD models in the future. Finally, organoids should be integrated with complex *in vitro* platforms and artificial intelligence to facilitate high-throughput compound screening, identification of therapeutic targets, and application of personalized medicine.

RESOURCE AVAILABILITY

Lead contact

Further information and requests for resources and reagents should be direct to and will be fulfilled by the lead contact, Dr. Yamin Zhang (5020200824@nankai.edu.cn).

Materials availability

This study did not generate new animals, cell lines, or unique reagents.

Data and code availability

- The raw data of RNA-seq datasets in this study have been deposited in the NCBI Sequence Read Archive, accession number: PRJNA1113135.
- This paper does not report original code.
- Any additional information for reanalyzing the data in this study is available from the lead contact upon request.

ACKNOWLEDGMENTS

This work was supported by the National Natural Science Foundation of China (82372194 and 82204546), the Tianjin Natural Science Foundation (21JCYBJ00050 and 21JCYBJC00320), and the Tianjin Health Science and Technology Project (TJWJ2021ZD002, TJWJ2023MS012, TJWJ2023QN034, and TJWJ2023QN028).

AUTHOR CONTRIBUTIONS

Conceptualization, Y.Z., L.Z., S.L., and W.T.; methodology, L.Z., P.H., Z.W., and T.Z.; software, L.W., P.H., and Z.W.; formal analysis and visualization, L.Z., S.L., and Y.Y.; data curation, L.W., T.Z., and Z.W.; writing – original draft, L.Z., S.L., and W.T.; writing – review and editing, Z.W., L.Y., T.C., and Y.Z.; supervision and project administration, T.C. and Y.Z.

DECLARATION OF INTERESTS

The authors declare no competing interests.

STAR★METHODS

Detailed methods are provided in the online version of this paper and include the following:

- KEY RESOURCES TABLE
- EXPERIMENTAL MODEL AND STUDY PARTICIPANT DETAILS
  - Liver tissues
  - Ethical approval
- METHOD DETAILS

SUPPLEMENTAL INFORMATION

Supplemental information can be found online at https://doi.org/10.1016/j.isci.2025.112344.

Received: May 18, 2024
Revised: November 5, 2024
Accepted: March 31, 2025
Published: April 3, 2025

REFERENCES

1. Rinella, M.E., Lazarus, J.V., Ratziu, V., Francque, S.M., Sanyal, A.J., Kanwal, F., Romero, D., Abdelmalek, M.F., Anstee, Q.M., Arab, J.P., et al. (2023). A multisociety Delphi consensus statement on new fatty liver disease nomenclature. J. Hepatol. *79*, 1542–1556. https://doi.org/10.1016/j.jhep.2023.06.003.
2. Ye, Q., Zou, B., Yeo, Y.H., Li, J., Huang, D.Q., Wu, Y., Yang, H., Liu, C., Kam, L.Y., Tan, X.X.E., et al. (2020). Global prevalence, incidence, and outcomes of non-obese or lean non-alcoholic fatty liver disease: a systematic review and meta-analysis. Lancet Gastroenterol. Hepatol. *5*, 739–752. https://doi.org/10.1016/S2468-1253(20)30077-7.
3. Berná, G., and Romero-Gomez, M. (2020). The role of nutrition in non-alcoholic fatty liver disease: Pathophysiology and management. Liver Int. *40*, 102–108. https://doi.org/10.1111/liv.14360.
4. Younossi, Z.M., Golabi, P., Paik, J.M., Henry, A., Van Dongen, C., and Henry, L. (2023). The global epidemiology of nonalcoholic fatty liver disease (NAFLD) and nonalcoholic steatohepatitis (NASH): a systematic review. Hepatology *77*, 1335–1347. https://doi.org/10.1097/HEP.0000000000000004.
5. Quek, J., Chan, K.E., Wong, Z.Y., Tan, C., Tan, B., Lim, W.H., Tan, D.J.H., Tang, A.S.P., Tay, P., Xiao, J., et al. (2023). Global prevalence of non-alcoholic fatty liver disease and non-alcoholic steatohepatitis in the overweight and obese population: a systematic review and meta-analysis. Lancet Gastroenterol. Hepatol. *8*, 20–30. https://doi.org/10.1016/S2468-1253(22)00317-X.
6. Younossi, Z., Tacke, F., Arrese, M., Chander Sharma, B., Mostafa, I., Bugianesi, E., Wai-Sun Wong, V., Yilmaz, Y., George, J., Fan, J., and Vos, M.B. (2019). Global Perspectives on Nonalcoholic Fatty Liver Disease and Nonalcoholic Steatohepatitis. Hepatology *69*, 2672–2682. https://doi.org/10.1002/hep.30251.
7. Loomba, R., Friedman, S.L., and Shulman, G.I. (2021). Mechanisms and disease consequences of nonalcoholic fatty liver disease. Cell *184*, 2537–2564. https://doi.org/10.1016/j.cell.2021.04.015.
8. Stefan, N., Häring, H.U., and Cusi, K. (2019). Non-alcoholic fatty liver disease: causes, diagnosis, cardiometabolic consequences, and treatment strategies. Lancet Diabetes Endocrinol. *7*, 313–324. https://doi.org/10.1016/S2213-8587(18)30154-2.
9. Ramos, M.J., Bandiera, L., Menolascina, F., and Fallowfield, J.A. (2022). In vitro models for non-alcoholic fatty liver disease: Emerging platforms and their applications. iScience *25*, 103549. https://doi.org/10.1016/j.isci.2021.103549.
10. Van Herck, M.A., Vonghia, L., and Francque, S.M. (2017). Animal Models of Nonalcoholic Fatty Liver Disease-A Starter's Guide. Nutrients *9*, 1072. https://doi.org/10.3390/nu9101072.
11. Wang, S.X., Yan, J.S., and Chan, Y.S. (2022). Advancements in MAFLD Modeling with Human Cell and Organoid Models. Int. J. Mol. Sci. *23*, 11850. https://doi.org/10.3390/ijms231911850.
12. Kim, J.H., Wang, M., Lee, J., Park, H.J., Han, C., Hong, H.S., Kim, J.S., An, G.H., Park, K., Park, H.K., et al. (2018). Prediction of hepatotoxicity for drugs using human pluripotent stem cell-derived hepatocytes. Cell Biol. Toxicol. *34*, 51–64. https://doi.org/10.1007/s10565-017-9392-y.
13. Sinton, M.C., Meseguer-Ripolles, J., Lucendo-Villarin, B., Wernig-Zorc, S., Thomson, J.P., Carter, R.N., Lyall, M.J., Walker, P.D., Thakker, A., Meehan, R.R., et al. (2021). A human pluripotent stem cell model for the analysis of metabolic dysfunction in hepatic steatosis. iScience *24*, 101931. https://doi.org/10.1016/j.isci.2020.101931.
14. Osonoi, S., and Takebe, T. (2024). Organoid-guided precision hepatology for metabolic liver disease. J. Hepatol. *80*, 805–821. https://doi.org/10.1016/j.jhep.2024.01.002.
15. Sun, X.C., Kong, D.F., Zhao, J., Faber, K.N., Xia, Q., and He, K. (2023). Liver organoids: established tools for disease modeling and drug development. Hepatol. Commun. *7*, e0105. https://doi.org/10.1097/HC9.0000000000000105.
16. Mun, S.J., Ryu, J.S., Lee, M.O., Son, Y.S., Oh, S.J., Cho, H.S., Son, M.Y., Kim, D.S., Kim, S.J., Yoo, H.J., et al. (2019). Generation of expandable human pluripotent stem cell-derived hepatocyte-like liver organoids. J. Hepatol. *71*, 970–985. https://doi.org/10.1016/j.jhep.2019.06.030.
17. Ouchi, R., Togo, S., Kimura, M., Shinozawa, T., Koido, M., Koike, H., Thompson, W., Karns, R.A., Mayhew, C.N., McGrath, P.S., et al. (2019). Modeling Steatohepatitis in Humans with Pluripotent Stem Cell-Derived Organoids. Cell Metab. *30*, 374–384.e6. https://doi.org/10.1016/j.cmet.2019.05.007.
18. Ramli, M.N.B., Lim, Y.S., Koe, C.T., Demircioglu, D., Tng, W., Gonzales, K.A.U., Tan, C.P., Szczerbinska, I., Liang, H., Soe, E.L., et al. (2020). Human Pluripotent Stem Cell-Derived Organoids as Models of Liver Disease. Gastroenterology *159*, 1471–1486.e12. https://doi.org/10.1053/j.gastro.2020.06.010.
19. Huch, M., Gehart, H., van Boxtel, R., Hamer, K., Blokzijl, F., Verstegen, M.M.A., Ellis, E., van Wenum, M., Fuchs, S.A., de Ligt, J., et al. (2015). Long-term culture of genome-stable bipotent stem cells from adult human liver. Cell *160*, 299–312. https://doi.org/10.1016/j.cell.2014.11.050.
20. Elbadawy, M., Yamanaka, M., Goto, Y., Hayashi, K., Tsunedomi, R., Hazama, S., Nagano, H., Yoshida, T., Shibutani, M., Ichikawa, R., et al. (2020). Efficacy of primary liver organoid culture from different stages of non-alcoholic steatohepatitis (NASH) mouse model. Biomaterials *237*, 119823. https://doi.org/10.1016/j.biomaterials.2020.119823.
21. McCarron, S., Bathon, B., Conlon, D.M., Abbey, D., Rader, D.J., Gawronski, K., Brown, C.D., Olthoff, K.M., Shaked, A., and Raabe, T.D. (2021). Functional Characterization of Organoids Derived From Irreversibly Damaged Liver of Patients With NASH. Hepatology *74*, 1825–1844. https://doi.org/10.1002/hep.31857.
22. Sorrentino, G., Rezakhani, S., Yildiz, E., Nuciforo, S., Heim, M.H., Lutolf, M.P., and Schoonjans, K. (2020). Mechano-modulatory synthetic niches for liver organoid derivation. Nat. Commun. *11*, 3416. https://doi.org/10.1038/s41467-020-17161-0.
23. Hendriks, D., Brouwers, J.F., Hamer, K., Geurts, M.H., Luciana, L., Massalini, S., López-Iglesias, C., Peters, P.J., Rodríguez-Colman, M.J., Chuva de Sousa Lopes, S., et al. (2023). Engineered human hepatocyte organoids enable CRISPR-based target discovery and drug screening for steatosis. Nat. Biotechnol. *41*, 1567–1581. https://doi.org/10.1038/s41587-023-01680-4.
24. Kimura, M., Iguchi, T., Iwasawa, K., Dunn, A., Thompson, W.L., Yoneyama, Y., Chaturvedi, P., Zorn, A.M., Wintzinger, M., Quattrocelli, M., et al. (2022). En masse organoid phenotyping informs metabolic-associated genetic susceptibility to NASH. Cell *185*, 4216–4232.e16. https://doi.org/10.1016/j.cell.2022.09.031.
25. Han, D.W., Xu, K., Jin, Z.L., Xu, Y.N., Li, Y.H., Wang, L., Cao, Q., Kim, K.P., Ryu, D., Hong, K., and Kim, N.H. (2023). Customized liver organoids as an

advanced in vitro modeling and drug discovery platform for non-alcoholic fatty liver diseases. Int. J. Biol. Sci. *19*, 3595–3613. https://doi.org/10.7150/ijbs.85145.

26. Liu, Y., Sheng, J.Y., Yang, C.F., Ding, J., and Chan, Y.S. (2023). A decade of liver organoids: Advances in disease modeling. Clin. Mol. Hepatol. *29*, 643–669. https://doi.org/10.3350/cmh.2022.0428.
27. Shi, S., Roest, H.P., van den Bosch, T.P.P., Bijvelds, M.J.C., Boehnert, M.U., de Jonge, J., Dekker, S.O., de Vries, A.A.F., de Jonge, H.R., Verstegen, M.M.A., and van der Laan, L.J.W. (2023). Modeling bile duct ischemia and reoxygenation injury in human cholangiocyte organoids for screening of novel cholangio-protective agents. EBioMedicine *88*, 104431. https://doi.org/10.1016/j.ebiom.2022.104431.
28. Wang, Z., Xing, C., van der Laan, L.J.W., Verstegen, M.M.A., Spee, B., and Masereeuw, R. (2024). Cholangiocyte organoids to study drug-induced injury. Stem Cell Res. Ther. *15*, 78. https://doi.org/10.1186/s13287-024-03692-6.
29. Li, N., Li, X., Ding, Y., Liu, X., Diggle, K., Kisseleva, T., and Brenner, D.A. (2023). SREBP Regulation of Lipid Metabolism in Liver Disease, and Therapeutic Strategies. Biomedicines *11*, 3280. https://doi.org/10.3390/biomedicines11123280.
30. Xu, S., Wu, X., Wang, S., Xu, M., Fang, T., Ma, X., Chen, M., Fu, J., Guo, J., Tian, S., et al. (2024). TRIM56 protects against nonalcoholic fatty liver disease by promoting the degradation of fatty acid synthase. J. Clin. Investig. *134*, e166149. https://doi.org/10.1172/JCI166149.
31. Li, Y., Huang, X., Yang, G., Xu, K., Yin, Y., Brecchia, G., and Yin, J. (2022). CD36 favours fat sensing and transport to govern lipid metabolism. Prog. Lipid Res. *88*, 101193. https://doi.org/10.1016/j.plipres.2022.101193.
32. Chen, Z., Tian, R., She, Z., Cai, J., and Li, H. (2020). Role of oxidative stress in the pathogenesis of nonalcoholic fatty liver disease. Free Radic. Biol. Med. *152*, 116–141. https://doi.org/10.1016/j.freeradbiomed.2020.02.025.
33. Powell, E.E., Wong, V.W.S., and Rinella, M. (2021). Non-alcoholic fatty liver disease. Lancet *397*, 2212–2224. https://doi.org/10.1016/S0140-6736(20)32511-3.
34. Harrison, S.A., Bedossa, P., Guy, C.D., Schattenberg, J.M., Loomba, R., Taub, R., Labriola, D., Moussa, S.E., Neff, G.W., Rinella, M.E., et al. (2024). A Phase 3, Randomized, Controlled Trial of Resmetirom in NASH with Liver Fibrosis. N. Engl. J. Med. *390*, 497–509. https://doi.org/10.1056/NEJMoa2309000.
35. Park, J., Rah, S.Y., An, H.S., Lee, J.Y., Roh, G.S., Ryter, S.W., Park, J.W., Yang, C.H., Surh, Y.J., Kim, U.H., et al. (2023). Metformin-induced TTP mediates communication between Kupffer cells and hepatocytes to alleviate hepatic steatosis by regulating lipophagy and necroptosis. Metabolism *141*, 155516. https://doi.org/10.1016/j.metabol.2023.155516.
36. Armstrong, M.J., Gaunt, P., Aithal, G.P., Barton, D., Hull, D., Parker, R., Hazlehurst, J.M., Guo, K., LEAN trial team; and Abouda, G., et al. (2016). Liraglutide safety and efficacy in patients with non-alcoholic steatohepatitis (LEAN): a multicentre, double-blind, randomised, placebo-controlled phase 2 study. Lancet *387*, 679–690. https://doi.org/10.1016/S0140-6736(15)00803-X.
37. Rinella, M., and Charlton, M. (2016). The globalization of nonalcoholic fatty liver disease: Prevalence and impact on world health. Hepatology *64*, 19–22. https://doi.org/10.1002/hep.28524.
38. Neuschwander-Tetri, B.A. (2020). Therapeutic Landscape for NAFLD in 2020. Gastroenterology *158*, 1984–1998.e3. https://doi.org/10.1053/j.gastro.2020.01.051.
39. Shiota, J., Samuelson, L.C., and Razumilava, N. (2021). Hepatobiliary Organoids and Their Applications for Studies of Liver Health and Disease: Are We There Yet. Hepatology *74*, 2251–2263. https://doi.org/10.1002/hep.31772.
40. Peiseler, M., Schwabe, R., Hampe, J., Kubes, P., Heikenwälder, M., and Tacke, F. (2022). Immune mechanisms linking metabolic injury to inflammation and fibrosis in fatty liver disease - novel insights into cellular communication circuits. J. Hepatol. *77*, 1136–1160. https://doi.org/10.1016/j.jhep.2022.06.012.
41. Barreby, E., Chen, P., and Aouadi, M. (2022). Macrophage functional diversity in NAFLD - more than inflammation. Nat. Rev. Endocrinol. *18*, 461–472. https://doi.org/10.1038/s41574-022-00675-6.
42. Hu, Y., Hu, X., Luo, J., Huang, J., Sun, Y., Li, H., Qiao, Y., Wu, H., Li, J., Zhou, L., and Zheng, S. (2023). Liver organoid culture methods. Cell Biosci. *13*, 197. https://doi.org/10.1186/s13578-023-01136-x.

STAR★METHODS

KEY RESOURCES TABLE

REAGENT or RESOURCE	SOURCE	IDENTIFIER
Antibodies		
Epcam	Proteintech	Cat# 66316-1-Ig; RRID: AB_2881697
CK19	Proteintech	Cat# 10712-1-AP; RRID: AB_2133325
ALB	Proteintech	Cat# 66051-1-Ig; RRID: AB_11042320
AAT	Proteintech	Cat# 66135-1-Ig; RRID: AB_2881534
E-cadherin	Proteintech	Cat# 60335-1-Ig; RRID: AB_2881444
HNF4A	Proteintech	Cat# 61190; RRID: AB_2793545
Goat Anti-Mouse IgG H&L (Alexa Fluor® 488)	Abcam	Cat# ab150113; RRID: AB_2576208
Goat Anti-Rabbit IgG H&L (Alexa Fluor® 594)	Abcam	Cat# ab150080
Biological samples		
Human liver tissue	Tianjin First Central Hospital	Table S1
Chemicals, peptides, and recombinant proteins		
Advanced DMEM/F-12	Thermo Fisher	Cat# 12634-010
GlutaMAX	Thermo Fisher	Cat# 35050061
HEPES	Thermo Fisher	Cat# 15630080
Penicillin/streptomycin	Thermo Fisher	Cat# 15140122
B27 supplement	Thermo Fisher	Cat# 17504044
N2 supplement	Thermo Fisher	Cat# 17502048
N-acetyl-L-cysteine	MedChemExpress	Cat# HY-B0215
Noggin	MedChemExpress	Cat# HY-P70558
Nicotinamide	MedChemExpress	Cat# HY-B0150
Gastrin I	MedChemExpress	Cat# HY-P1097
A83-01	MedChemExpress	Cat# HY-10432
Forskolin	MedChemExpress	Cat# HY-15371
R-spondin 1	R&D Systems	Cat# 4645-RS
Y-27632	Stemcell	Cat# 72304
Wnt3a	MedChemExpress	Cat# HY-P70453B
DAPT	MedChemExpress	Cat# HY-13027
Dexamethasone	MedChemExpress	Cat# HY-14648
BMP7	MedChemExpress	Cat# HY-P7008
EGF	novoprotein	Cat# C029
FGF10	novoprotein	Cat# CR11
HGF	novoprotein	Cat# CJ72
FGF19	novoprotein	Cat# CG74
Collagenase IV	Solarbio	Cat# 9001-12-1
BME (Cultrex Basement Membrane Extract, Type 2)	R&D Systems	Cat# 3532-010-02
Cell Recovery Solution	Corning	Cat# 354253
TrypLE	Thermo Fisher	Cat# 12604021
Indocyanine green	MedChemExpress	Cat# HY- D0711
Nile Red	MedChemExpress	Cat# HY-D0718
IGEPAL® CA-630	Beyotime	Cat# ST2045
H2DCFDA	MedChemExpress	Cat# HY-D0940
Oleic acid	MedChemExpress	Cat# HY-N1446
Metformin	MedChemExpress	Cat# HY-B0627
Liraglutide	MedChemExpress	Cat# HY-P0014

(*Continued on next page*)

Continued

REAGENT or RESOURCE	SOURCE	IDENTIFIER
Obeticholic acid	MedChemExpress	Cat# HY-12222
Elafibranor	MedChemExpress	Cat# HY-16737
Saroglitazar	MedChemExpress	Cat# HY-19937
Critical commercial assays		
Periodic Acid Schiff (PAS) Stain Kit	Solarbio	Cat# G1281
Human Albumin ELISA kit	Abcam	Cat# ab179887
Human alpha 1 Antitrypsin ELISA Kit	Abcam	Cat# ab108799
Human IL-6 ELISA Kit	Abcam	Cat# ab178013
Triglyceride Assay Kit	Abcam	Cat# ab63556
CellTiter-Glo® 3D Cell Viability Assay	Promega	Cat# G9682
TransZol Up Plus RNA Kit	TransGen Biotech	Cat# ER501-01-V2
Transcriptor First Strand cDNA Synthesis Kit	Roche	Cat# 04897030001
FastStart Universal SYBR Green Master (Rox)	Roche	Cat# 04913914001
Deposited data		
RNA-Sequencing Data	This paper	PRJNA1113135
Experimental models: Cell lines		
Human liver tissue-derived cells	This paper	N/A
Oligonucleotides		
See Table S3	This paper	N/A
Software and algorithms		
GraphPad Prism 8.0.2	GraphPad	https://www.graphpad.com/
Fiji-image J	open source	https://imagej.net/software/fiji/
FlowJo_v10.8.1	BD Biosciences	https://www.flowjo.com/
R 3.6.2	S. Urbanek & H.-J. Bibiko	http://www.R-project.org
Leica Application Suite X	Leica	https://www.leica-microsystems.com.cn/

EXPERIMENTAL MODEL AND STUDY PARTICIPANT DETAILS

Liver tissues

Liver tissues were obtained from patients who underwent partial liver resection due to liver trauma in Tianjin First Central Hospital, and the detailed clinical information of the patients was presented in Table S1.

Ethical approval

The Medical Ethics Committee of Tianjin First Central Hospital approved the use of these tissues for research purposes (2020N221KY), and informed consent was obtained from the patients.

METHOD DETAILS

Human LOs initiation and culture

As previously described, the liver tissues were cut into pieces of roughly 0.5 mm^3, washed with phosphate-buffered saline (PBS) and digested with collagenase IV at 37°C for approximately 30 minutes.[19] The resulting suspension was filtered through a 70 μm cell strainer and centrifuged at 300g, 4°C for 5 minutes. After cell counting, the cell suspension needed were calculated according to the planting density and centrifuged again. The cell pellet was mixed with BME (Basement Membrane Extract, Type 2) quickly and plant the droplets in a 24-well plate at the density of 20,000-30,000 cells per well (50 μl BME). After BME was solidified, organoid initiating medium (OIM) was added and changed every 3 days. COs were formed after 5-7 days and could be mechanically dissociated into fragments for passage. Subsequently, the medium was substituted with organoid growth medium (OGM). Once the diameter of the COs reached 300-500 μm, they could be passaged again, cryopreserved, or collected for analysis. When COs needed to be differentiated, organoid differentiation medium (ODM) was added after 3 days of passage, and fresh medium was provided every 2-3 days. Differentiated LOs could be obtained after 10 days for analysis or subsequent experiments. Table S2 listed the composition of OIM, OGM, and ODM.[42]

H&E and immunofluorescence

Organoids were collected, fixed in 4% paraformaldehyde (PFA) at room temperature (RT) for 1 hour, re-suspended in 3% agarose solution and solidified on ice, then dehydrated, embedded in paraffin, and sliced at 3 μm. H&E was performed after de-waxing and rehydration. For immunofluorescence, the slides were de-waxing and subjected to antigen retrieval with EDTA, membrane permeabilization with 0.5% Triton, blocked with 3% BSA, and then incubated with diluted primary antibody overnight at 4°C. After washed in PBST, slides were incubated with diluted secondary antibody for 2 hours at RT and sealed with tablets containing DAPI after a final wash. All images were acquired using a Total internal reflection fluorescent microscope TIRF&Thunder (Leica).

Functional analysis of LOs

For detection of glycogen accumulation in liver organoids, Periodic acid-Schiff (PAS) staining was performed on slides of LOs. For the uptake and release of indocyanine green (ICG), LOs were incubated with 1 mg/ml ICG for 15 minutes at 37°C and 5% CO_2. The organoids were collected and ICG uptake images were taken under a microscope. Then the organoids were washed gently 3 times with PBS and fresh medium was added. After incubation for 1 hour at 37°C and 5% CO_2, images of ICG release were taken. For quantification of albumin (ALB) and Alpha-1-Antitrypsin (AAT) producted by LOs, the medium was collected 48 hours after each change of medium and analyzed using the human ALB elisa kit and human AAT elisa kit according to the manufacturer's instructions.

RNA extraction and RT-qPCR

Total RNA of organoids was extracted and purified using a TransZol Up Plus RNA Kit according to the manufacturer's instructions, and the quantity and quality of RNA were determined through NanoDrop spectrophotometry. Using the Transcriptor First Strand cDNA Synthesis Kit, RNA was reverse transcribed into single-stranded cDNA, which could be used directly for subsequent PCR with gene-specific primers. RT-qPCR was conducted using FastStart Universal SYBR Green Master (ROX) in conjunction with a real-time PCR instrument, appropriate PCR primers, and a hydrolysis probe. GAPDH was used as a housekeeping gene, and mRNA levels were normalized. A list of forward and reverse primer sequences was provided in Table S3.

RNA-sequencing and analysis

For 3 cases of organoids derived from different patients, we collected COs and LOs of different passages (including low, middle, and high passages). Total RNA of organoids was extracted follow the above method and the high-quality RNA samples were subsequently submitted to the Sangon Biotech (Shanghai) Co., Ltd. for library preparation and sequencing. Sequencing libraries were generated using VAHTSTM mRNA-seq V2 Library Prep Kit for Illumina® following manufacturer's recommendations and index codes were added to attribute sequences to each sample. The libraries were then quantified and pooled. Paired-end sequencing of the library was performed on the NovaSeq sequencers (Illumina, San Diego, CA). FastQC was used for evaluating the quality of sequenced data. Clean reads were mapped to the reference genome by HISAT2 with default parameters. Gene expression values of the transcripts were computed by StringTie. DESeq2 was used to determine differentially expressed genes (DEGs) between two samples. Genes were considered as significant differentially expressed if P-value ≤ 0.05 and $|\text{FoldChange}| \geq 2$. Functional enrichment analyses including Gene Ontology (GO) and Kyoto Encyclopedia of Genes and Genomes (KEGG) were performed to identify which DEGs were significantly enriched in GO terms or metabolic pathways. And Gene set enrichment analysis (GSEA) was performed using the R package clusterProfiler.

Construction and characterization of hepatic steatosis model

The COs were subcultured in 24-well plate or 96-well plate and then added to OGM medium. After 3 days of culture, the culture medium was changed to ODM medium, and fresh medium was subsequently changed every 2-3 days. After 10 days of differentiation, the medium was replaced with ODM containing different concentrations of OA (including 0, 200, 400, 600 and 800 μM).[17] The LOs were treated with OA for 3 days and collected to determine the optimal concentration of OA for constructing hepatic steatosis model, and the model was characterized as follows:

Lipid staining

The organoids were collected and fixed with 4% PFA. Subsequently, 1 μM Nile Red was added, and the samples were incubated at RT for 10 minutes and then washed twice with PBS and added DAPI to counterstain nuclei. The organoids were suspended in PBS and then observed and photographed using a Total internal reflection fluorescent microscope TIRF&Thunder (Leica). Image J software was used to measure fluorescence intensity of Nile Red.

Triglyceride content analysis

The organoids were collected and added 5% IGEPAL® CA-630 (Nonidet P-40 Substitute). Slowly heated the samples to 100°C for 3 minutes until the solution becomes cloudy, followed by cooling to RT. This step was repeated to ensure complete solubilization of all triglycerides. Subsequently, the samples were centrifuged at 20000g for 2 minutes using a microcentrifuge, and the supernatant was transferred to a new tube. The Triglyceride Assay Kit was used to determined the triglyceride concentration of the hepatic steatosis model according to the manufacturer's instructions.

Cell viability measurement

The CellTiter-Glo®3D Cell Viability Assay was used to assess cell viability. Briefly, the culture medium of organoids cultured in opaque 96-well assay plates was aspirated, followed by the addition of 100 μl of assay reagent and an equal volume of fresh culture

medium. The contents were thoroughly mixed for 5 minutes to induce cell lysis, and then incubated at RT for 30 minutes. A microplate reader was employed to quantify the ATP chemiluminescence signal and normalize the detection value as a percentage relative to the blank control group.

Reactive oxygen species analysis

The organoids were incubated with PBS solution containing 5 μM H2DCFDA for 30 minutes at 37°C in the dark. Some of organoids were digested with Tryple and the resulting cells were harvested, suspended in PBS, and promptly subjected to flow cytometric to determine the proportion of reactive oxygen species (ROS) positive cells. Additionally, certain organoids underwent counterstaining with DAPI and were observed under a Total internal reflection fluorescent microscope TIRF&Thunder (Leica).

RNA extraction and RT-qPCR

The method of RNA extraction and RT-qPCR was the same as before.

Drug screening

For the drug screening of hepatic steatosis model, metformin and several drugs already undergoing clinical trials to treat MASLD were employed, including liraglutide, obeticholic acid, elafibranor, and saroglitazar. Following the determination of the optimal concentration of OA for model construction through preliminary experiments, LOs were exposed to OA for a duration of 3 days, concomitantly with the addition of the aforementioned five drugs. Subsequently, the organoids were harvested for lipid staining, triglyceride content analysis, and cell viability assessment to ascertain the effect of the drugs. All drugs were procured from MedChemExpress, with their concentrations determined based on previously published literature: metformin at 100 μM, liraglutide at 20 μM, obeticholic acid at 10 μM, elafibranor at 50 μM, and saroglitazar at 25 μM.

QUANTIFICATION AND STATISTICAL ANALYSIS

Statistical analysis

All statistical analyses were performed using GraphPad Prism (version 8.3.0) and R software (version 3.6.2). Data were presented as the mean ± SD for at least three samples. Single comparisons between two independent datasets were performed using an unpaired Student's t-test. Multiple comparisons across one variable were carried out using a one-way analysis of variance (ANOVA). $P < 0.05$ was considered statistically significant.